Aalborg Universitet

AALBORG UNIVERSITY
DENMARK

Exploring Decentralized Ammonia Synthesis for Hydrogen Storage and Transport: A Comprehensive CFD Investigation with Experimental Validation and Parametric Study

Gu, Tianbao; Simon Araya, Samuel; Yin, Chungen; Liso, Vincenzo

Published in:
Energy Conversion and Management

DOI (link to publication from Publisher):
10.1016/j.enconman.2023.117604

Creative Commons License
CC BY 4.0

Publication date:
2023

Document Version
Publisher's PDF, also known as Version of record

Link to publication from Aalborg University

Citation for published version (APA):
Gu, T., Simon Araya, S., Yin, C., & Liso, V. (2023). Exploring Decentralized Ammonia Synthesis for Hydrogen Storage and Transport: A Comprehensive CFD Investigation with Experimental Validation and Parametric Study. *Energy Conversion and Management*, *295*, [117604]. https://doi.org/10.1016/j.enconman.2023.117604

General rights
Copyright and moral rights for the publications made accessible in the public portal are retained by the authors and/or other copyright owners and it is a condition of accessing publications that users recognise and abide by the legal requirements associated with these rights.

- Users may download and print one copy of any publication from the public portal for the purpose of private study or research.
- You may not further distribute the material or use it for any profit-making activity or commercial gain
- You may freely distribute the URL identifying the publication in the public portal -

Take down policy
If you believe that this document breaches copyright please contact us at vbn@aub.aau.dk providing details, and we will remove access to the work immediately and investigate your claim.

Energy Conversion and Management 295 (2023) 117604

Contents lists available at ScienceDirect

Energy Conversion and Management

journal homepage: www.elsevier.com/locate/enconman

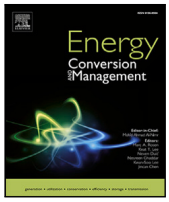

Exploring decentralized ammonia synthesis for hydrogen storage and transport: A comprehensive CFD investigation with experimental validation and parametric study

Tianbao Gu [a,*], Samuel Simon Araya [a], Chungen Yin [a], Vincenzo Liso [a]

[a] AAU Energy, Aalborg University, Pontoppidanstræde 111, Aalborg Øst, 9220, Nordjylland, Denmark

ARTICLE INFO

Keywords:
Hydrogen storage
Ammonia synthesis
CFD
Kinetic model
Ruthenium catalyst

ABSTRACT

Hydrogen energy plays a vital role in the transition towards a carbon-neutral society but faces challenges in storage and transport, as well as in production due to fluctuations in renewable electricity generation. Ammonia (NH_3), as a carbon-neutral hydrogen carrier, offers a promising solution to the energy storage and transport problem. To realize its potential and support the development of a hydrogen economy, exploring NH_3 synthesis in a decentralized form that integrates with distributed hydrogen production systems is highly needed. In this study, a computational fluid dynamics (CFD) model for the Ruthenium (Ru) catalysts-based Haber–Bosch reactor is developed. First, a state-of-the-art kinetic model comprehensively describing the complex catalytic reaction is assessed for its sensitivity and applicability to temperature, pressure and conversion. Then, the kinetic model is integrated into the CFD model, and its accuracy is verified through comparison with experimental data obtained from different Ru-based catalysts and operation conditions. Detailed CFD results for a given case are presented, offering a visual understanding of thermal gradients and species distributions inside the reactor. Finally, a CFD-based parametric study is performed to reveal the impacts of key operation parameters and optimize the NH_3 synthesis reactor. The results show that the NH_3 production rate is predominantly influenced by temperature, with a two-fold difference observed for every 30 °C variation, while pressure primarily affects the equilibrium. Additionally, the affecting mechanism of space velocity is thoroughly discussed and the best value for efficient NH_3 synthesis is found to be 180,000 h^{-1}. In conclusion, the CFD model and simulation results provide valuable insights for the design and control of decentralized NH_3 synthesis reactor and operation, contributing to the advancement of sustainable energy technologies.

1. Introduction

Driven by the Net Zero Emissions (IEA. [1]), hydrogen energy has been receiving remarkable interest as it is one of the most promising alternatives to carbon-intensive fuels while providing a potential solution for renewable electricity integration. Despite numerous policies for hydrogen economy being issued and technical difficulties being resolved, the utilization of hydrogen is still facing substantial challenges in storage and transport due to its low volumetric energy density and boiling point (−252.8 °C) [2]. Therefore, hydrogen economy always functions with a Power-to-X ('X' as an energy carrier) versatile system that produces hydrogen from power and converts the produced hydrogen to other chemicals, which are easy to be stored and transported such as ammonia (NH_3) and methanol. Different from hydrogen, ammonia has many desirable properties, for instance high energy density, carbon-free content, high hydrogen capacity (17.6 wt.%), and easy to store and transport (boiling point −33.8 °C) [3], making it very promising in long term and large scale storage and transport. Recently, Power-to-Ammonia is concluded as the best solution in [4], comprehensively considering the energy density, hydrogen capacity, cost of storage and transport, existing infrastructures and so on. Apart from being hydrogen carrier, NH_3 is also widely used in various sectors, e.g., producing fertilizers, as carbon-free fuel for engines, turbines and fuel cells [5]. It is playing a vital role in agriculture and industry and shows great potential in the energy sector to promote sustainable energy development and achieve carbon-neutral society [6]. The global production of NH_3 is estimated approximately 176 million metric tonnes per year and to be increased by 2.3% annually [7,8].

Currently, NH_3 is mainly produced by the well-known Haber–Bosch synthesis process (>96%) [7], in which hydrogen and nitrogen are used as the reactants at high temperature and pressure in the presence of catalyst (typically iron-based, recently Ruthenium-based) [9]. It is a complex heterogeneous catalytic process, including adsorption and

* Corresponding author.
E-mail address: tig@energy.aau.dk (T. Gu).

https://doi.org/10.1016/j.enconman.2023.117604
Received 19 June 2023; Received in revised form 7 August 2023; Accepted 28 August 2023
Available online 6 September 2023
0196-8904/© 2023 The Author(s). Published by Elsevier Ltd. This is an open access article under the CC BY license (http://creativecommons.org/licenses/by/4.0/).

Nomenclature

Acronyms

CFD	Computational fluid dynamics
$GHSV$	Gas hourly space velocity
Re	Reynolds number

Greek Letters

ϵ	Bed porosity (–)
η	Conversion of the limiting reactant (–)
Γ	Diffusion coefficient of transport equation
γ	Equivalent coefficient for calculating the time factor (–)
$\lambda(q)$	Stoichiometric parameter, 1 or 1.2 for H_2/N_2 feed ratio 3 or 1.5 (–)
μ	Fluid viscosity (Pa s)
ϕ	General variable in transport equations
Φ_i	Fugacity coefficients of ith species, NH_3, H_2 or N_2 (–)
ρ	Density ($kg\,m^{-3}$)
τ	Time factor (h^{-1})

Roman Symbols

$\vec{v}$	Fluid velocity vector ($m\,s^{-1}$)
A	Dimensionless pre-exponential factor of the kinetic constant (–)
a_{H_2}	H_2 species activity (–)
a_{N_2}	N_2 species activity (–)
a_{NH_3}	NH_3 species activity (–)
C	Inertial resistance coefficient of the porous bed (m^{-1})
D	Viscous resistance coefficient of the porous bed (m^{-2})
E_a	Activation energy for kinetic constant ($kcal\,kmol^{-1}\,K^{-1}$)
E_f	Total fluid energy (kJ)
h	Enthalpy of fluid (kJ)
k	Kinetic constant of the modified Temkin model ($mol\,h^{-1}\,dm^{-3}_{cat.}$)
K_a	Equilibrium constant of the synthesis reaction (–)
k_{eff}	Effective thermal conductivity of the catalyst bed ($W\,m^{-1}\,K^{-1}$)
K_{H_2}	Adsorption equilibrium constant of H_2 (–)
K_{NH_3}	Adsorption equilibrium constant of NH_3 (–)
P	Pressure (Pa/bar/atm)
q	Initial mole ratio of H_2 to N_2 (–)
R	Universal gas constant ($8.3145\,J\,K^{-1}\,mol^{-1}$)
r_{NH_3}	NH_3 production rate ($kg\,m^{-3}_{cat}\,h^{-1}$)
S	Source term for the solved transport equations
T	Temperature (K)
t	Time (s^{-1})
X_i	Mole fraction of ith species, NH_3, H_2 or N_2 (–)
Y_{NH_3}	NH_3 mass fraction (–)

desorption of H_2, N_2 and NH_3 on the catalyst surface, and limited by the inhibition of produced NH_3 [10]. Overall, NH_3 synthesis is an exothermic and reversible reaction, in which the high temperature (300–550 °C) is required to overcome the chemical bond energy, and high pressure (15–30 MPa) favors the equilibrium as well as the reaction rate [11]. In this scenario, the NH_3 synthesis plants are highly energy intensive and normally centralized with high amounts of carbon emissions. The existing NH_3 synthesis plants in the world contribute about 1.4% percent carbon dioxide (CO_2) emissions in total [12], and consume 2% percent of the world's annual primary energy supply, which are considered very huge [13]. Therefore, the attempts for reducing the energy consumption and carbon emissions of NH_3 synthesis are very necessary.

As many studies have reported, Ruthenium (Ru) is more active than Iron (Fe) for NH_3 production, the same conversion of the Haber–Bosch process can be achieved at lower temperature and pressure for Ru other than Fe [14,15]. Moreover, the advanced Ru-based catalysts require less thermal mass in synthesis reactor, enabling the decentralized unit to synthesize NH_3, which is very promising to be used for green hydrogen storage and transport. Thus, the modern Ru-based catalysts are recognized as the second generation catalysts for NH_3 synthesis with potential to reshape the typical Haber–Bosch process towards a more energy-efficient process [16,17]. In order to reveal the complex reaction mechanism and describe the process of NH_3 synthesis on Ru-based catalyst, several modeling work and numerical studies have been carried out. For example, the macroscopic kinetic models for Ru-based catalyst have been conducted, to express the conversion process and predict NH_3 production [15,18]. Among them, the modified Temkin model is considered as the up-to-date kinetic expression, comprehensively describing the adsorption and dissociation steps of the catalytic reaction [19,20]. Subsequently, the kinetics have been evaluated by fitting the modified Temkin expression to experimental data for various Ru-based catalysts, e.g., for the promoted Ru/C catalyst [19].

On the other hand, the computational fluid dynamics (CFD) modeling work, which can predict the details inside the reactor and optimize the reactor design and operation [21], is not adequate with respect to the kinetic modeling study. Only a few studies can be found in literature, for instance, Amin et al. [22] developed a two-dimensional (2D) CFD model for a Fe-based catalyst reactor of NH_3 synthesis, integrating the typical Temkin kinetic model to predict the catalytic reaction. The catalyst beds synthesizing NH_3 are assumed as uniform porous media, where the Brinkman equation is applied to model the fluid flow. The simulation results provide useful recommendations for the configuration design of the reactor. Another 2D simulation has been performed in ANSYS Fluent to validate a self-developed model and analyze a three-beds ammonia reactor. It is also a good attempt for implementing CFD into investigation of NH_3 synthesis [23]. While, to the best of the authors' knowledge, the CFD simulation incorporating the up-to-date kinetic model for Ru-based catalyst reactors of NH_3 synthesis has not been conducted. And it is believed that the CFD modeling study would facilitate the research on advanced NH_3 synthesis and promote its applications based on modern Ru-catalysts.

The motivation of this work is to explore decentralized NH_3 synthesis for better store and transport green hydrogen. The advanced Ru-based catalyst, which can be efficiently operated in mild conditions with less thermal mass, is intended to be used to enable the compact Haber–Bosch reactor. The objective of this paper is to develop a comprehensive CFD model implementing the up-to-date kinetic expression to simulate a small-scale NH_3 synthesis reactor over Ru-based catalyst. The performance of the kinetic model (modified Temkin model) in terms of pressure, temperature and conversion is assessed first. Then the CFD simulation results have been compared with 94 experimental cases in total for validation, which show good agreements. Subsequently, an in-depth case analysis has been made based on the modeling results, showing the inner species distributions and thermal gradients of the reactor. At last, two parametric studies with

respect to temperature, pressure and space velocity have been conducted, revealing the sensitivities to the key parameters, suggesting the best operation conditions and providing meaningful insights for the Ruthenium catalyst-based Haber–Bosch NH_3 synthesis. This CFD modeling study is advanced in reliability and applicability, which can serve as a powerful tool to transit NH_3 synthesis to an energy-saving, low carbon emission and compact process.

2. Modeling description

2.1. Kinetic model

NH_3 synthesis is a complex catalytic process, which undergoes several adsorption and dissociation steps at the catalyst surface [24]. In order to simplify the NH_3 synthesis process in CFD simulation, the global reaction mechanism is assumed as follows [22].

$$0.5N_2 + 1.5H_2 \Leftrightarrow NH_3 \qquad \Delta H = -46.22\,\mathrm{kJ/mol\,NH_3} \tag{1}$$

The corresponding macroscopic kinetic model describing the conversion rate is normally governed by a complex functions in terms of temperature, pressure and species, considering the surface coverage and material structure [20]. The most well-known kinetic model for NH_3 synthesis using Ru-based catalyst is the modified Temkin model, which describes the unique features of the catalytic reaction with Ru element, as expressed in Eq. (2) [19].

$$\frac{d\eta}{d\tau} = k\lambda(q)\frac{(a_{N_2})^{0.5}\left[\frac{(a_{H_2})^{0.375}}{(a_{NH_3})^{0.25}}\right] - \frac{1}{K_a}\left[\frac{(a_{NH_3})^{0.75}}{(a_{H_2})^{1.125}}\right]}{1 + K_{H_2}(a_{H_2})^{0.3} + K_{NH_3}(a_{NH_3})^{0.2}} \tag{2}$$

Here $d\eta/d\tau$ denotes the consumption rate of limiting reactant ($\mathrm{mol\,h^{-1}\,dm^{-3}_{cat.}}$), K_a indicates the equilibrium constant, k represents the kinetic constant with respect to the species activities (a_{NH_3}, a_{H_2} and a_{N_2}) [25,26], $\lambda(q)$ is the stoichiometric parameter, i.e., 1 or 1.2 when the $q = H_2/N_2$ mole feeding ratio is 3 or 1.5, respectively [27]. The adsorption equilibrium constants of reactants K_{H_2} and K_{NH_3} are expressed below [20],

$$log_e K_{H_2} = -\frac{56.9024}{R} + \frac{37656}{RT} \tag{3}$$

$$log_e K_{NH_3} = -\frac{34.7272}{R} + \frac{29228}{RT} \tag{4}$$

where R is the universal gas constant (8.3145 $\mathrm{J\,mol^{-1}K-1}$). The equilibrium constant K_a and the kinetic constant k are defined as [26]:

$$log_{10}K_a = -2.691122log_{10}T - 5.519265\times10^{-5}T + 1.848863\times10^{-6}T^2 + 2001.6/T + 2.689 \tag{5}$$

$$k = A\exp(-\frac{E_a}{RT}) \tag{6}$$

where the kinetic parameters for Ru/C catalyst are investigated in [19], i.e., the dimensionless pre-exponential factor $A = 9.02\times10^8$ and the activation energy $E_a = 23.0\ \mathrm{kcal\,kmol^{-1}K^{-1}}$, which are used in this numerical study. The kinetic constant is an exponential function with respect to temperature, indicating the sensitivity of the reaction rate to temperature. The activity of the ith species (NH_3, H_2 or N_2) a_i can be calculated as follows,

$$a_i = X_i\Phi_i P \tag{7}$$

where P indicates the total pressure (atm), X_i and Φ_i denote the mole fraction and fugacity coefficient of ith species, respectively. The fugacity coefficients for the reactants and product are fitted by temperature (kelvin) and pressure (atm) using the following equations [28].

$$\Phi_{N_2} = 0.93431737 + 0.2028538\times10^{-3}T + 0.2958961\times10^{-3}P - 0.270727148\times10^{-6}T^2 + 0.4775207\times10^{-6}P^2 \tag{8}$$

$$\Phi_{H_2} = \exp\{\exp(-0.38402T^{0.125} + 0.541)P - \exp(-0.1263T^{0.5} - 15.98)P^2 + 300\exp(-0.011901T - 5.941)\times\exp(-P/300)\} \tag{9}$$

$$\Phi_{NH_3} = 0.1438996 + 0.2028538\times10^{-2}T - 0.4487672\times10^{-3}P - 0.1142945\times10^{-5}T^2 + 0.2761216\times10^{-6}P^2 \tag{10}$$

It is worth mentioning that, the time factor $\tau\ \mathrm{h^{-1}}$ is defined as the catalyst volume per Gas Hourly Space Velocity (GHSV), i.e., the inlet volumetric gas flow rate per volume of the catalyst bed $\mathrm{h^{-1}}$, as presented in Eq. (11).

$$\tau = \frac{litres\ of\ catalyst}{N_2\ (q=3)\ or\ H_2(q=1.5)\ feeding\ rate\ \frac{mol}{h}} = \frac{22.414}{GHSV\times\gamma} \tag{11}$$

Since the reaction rate (Eq. (2)) is defined as the limiting reactant (either N_2 or H_2)N, the equivalent coefficient is set to $\gamma = 0.25$ (1 mol N_2/4 mol) or 0.6 (1.5 mol H_2/2.5 mol) for $q = 3$ or 1.5, respectively [19]. Thus, the ammonia production rate is slightly different due to the ratio of H_2/N_2 in the feeding flow. Finally, the fractional conversion of the limited reactant vs. reaction time is derived as follows.

$$\frac{d\eta}{dt} = k\lambda(q)\gamma\frac{(a_{N_2})^{0.5}\left[\frac{(a_{H_2})^{0.375}}{(a_{NH_3})^{0.25}}\right] - \frac{1}{K_a}\left[\frac{(a_{NH_3})^{0.75}}{(a_{H_2})^{1.125}}\right]}{1 + K_{H_2}(a_{H_2})^{0.3} + K_{NH_3}(a_{NH_3})^{0.2}}\cdot\frac{GHSV}{22.414} \tag{12}$$

This is the final equation integrated into the CFD framework to calculate the reaction rate, in which GHSV is used to quantify the overall conversion rate instead of catalyst amount. Thus the impacts of the single factor of residence time or the catalyst bed volume on the conversion for the same GHSV are largely reduced, theoretically strengthening the model's applicability. For more details of the modified Temkin kinetic model of NH_3 synthesis refer to [19,20].

2.2. CFD simulation

2.2.1. Simulated reactor and experimental data

To verify the model's reliability and applicability, a lab-scale reactor has been simulated and compared with the corresponding experimental data. The catalyst bed with 12 mm diameter and 40 mm length is located in the center of the reactor tube, as shown in Fig. 1. The initial reactants, i.e., H_2 and N_2, are supplied from the top, and the syn-gas flows out from the bottom.

The experimental data used for validation in this study are obtained in [19] using Ru/C catalyst. The experiments are carried out initially for developing a kinetic model, therefore, several specific settings have been made. For instance, the loaded catalyst in the reactor is diluted by quartz powder (catalyst to quartz volumetric ratio is 1/32) to keep the reaction zone approximately isothermal, while resulting in the catalyst bed very long (400 mm). All the experimental tests are accomplished under iso-thermal condition such as 430 °C. However, these specific settings do not generally fit a full lab-scale demonstrator of NH_3 synthesis, neither CFD simulation. Thus, the reactor simulated in this study is not completely the same as the one used for outputting the experimental data, several modifications have been made to meet the general code of a lab-scale demonstrator. For example, the catalyst bed is assumed only filled by catalysts, which largely shorten the length of the bed. Meanwhile to maintain the equivalent fluid properties, the flow rate is calculated based on the GHSV with the same dilution ratio used in the experiments. The catalyst bed is heated up by side walls, thus the lab-scale reactor is not fully isothermal in practice. Therefore, both isothermal simulation and non-isothermal simulation have been performed, of which the former is mainly for model validation and the latter is for more substantial analysis. Apart from these modifications, other operation parameters, e.g., pressure, particle size, etc., of the simulation case are consistent with the experiments. For more details on the experimental data refer to [19].

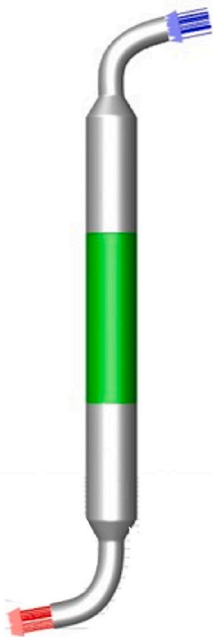

Fig. 1. Geometry of the lab-scale reactor for NH_3 synthesis.

Table 1
Mesh quality assessment of several key indexes.

Criteria	Value
Total cell number	314,160
Equiangle skewness	0–0.3: 94.37%
(0–0.3 very high, 0.3–0.5 high, 0.5–0.8 acceptable)	0.3–0.5: 5.17%
	0.5–0.7: 0.46%
Aspect ratio	1–1.95: 34.67%
(≃ 1 best, <5 good, can be bigger for inflation layers)	1.95–4.8: 44.7%
	4.8–6.7: 14.66%
	6.7–10.4: 5.97%
Jacobian determinant (0–1, >0.2 is good)	>0.53

Table 2
Summary of the numerical methods used in this CFD model.

Items	Numerical methods used
Catalyst bed	Non-laminar porous zone with fixed porosity, particle size and source terms[a]
Turbulence	SST $k-\omega$ model
Chemical reaction	$0.5N_2 + 1.5H_2 = NH_3$
Kinetic rate	The modified Temkin model, using Expressions in Fluent to integrate it
Boundary conditions	Mass flow inlet[b]; pressure outlet
Numerical methods	Coupled algorithm enabling pseudo transient; second order upwind scheme for discretization.

[a] Self-defined expressions for sources terms due to the catalytic reaction.

[b] Set 0.001 NH_3 as the minimum mole fraction to achieve CFD convergence [29].

2.2.2. CFD framework

The catalyst bed is assumed as a porous zone, where the ammonia synthesis takes place through the catalyst layers [29,30]. In this work, a three-dimensional (3D) steady state CFD model describing the turbulent flow through the porous medium with catalytic reaction is developed, in which the below assumptions are used.

- The particle size is uniform and the porosity is isotropic in the catalyst bed.
- The solid and gas phases in the same cell are in thermal equilibrium, i.e., the two phases share the same temperature [31].
- Only three species: NH_3, H_2 and N_2 exist in the reactor, regardless of the radicals, and the mixture gas follows the ideal gas law [23].
- The volumetric homogeneous reactions other than the global reaction mechanism in the pores are neglected [32].

The general governing equation for modeling the steady state fluid flow inside the porous catalyst bed is expressed as follows [33].

$$\nabla \cdot (\rho_f \vec{v}\phi) = \nabla \cdot (\varepsilon \Gamma \nabla \phi) + \varepsilon S_\phi \tag{13}$$

where ε denotes the bed porosity, ρ_f represents the fluid density, $\vec{v}$ indicates the velocity vector, ϕ and S_ϕ denote the general variable (mass, velocity, species and turbulence) and its corresponding source term, respectively. Among them, the additional source term for momentum equation is modeled by the description of a viscous term and an inertial loss term in the porous zone as presented:

$$S_i = -\left(\sum D_{ij}\mu v_j + \sum C_{ij}\frac{1}{2}\rho_f |v| v_j\right) \tag{14}$$

where S_i is the source term for the ith (x, y, z) momentum equation, the key parameters, i.e., prescribed matrices viscous resistance D and inertial resistance C, are calculated by the Ergun equation [34]. Here the uniform porosity and particle diameter of 0.4 and 0.2 mm, respectively, are used in this model. The density of the gas mixture is updated by the ideal gas law.

The solid phase and fluid phase in the porous catalyst zone are assumed to be in thermal equilibrium, thus a lumped energy equation is solved in the porous zone [33].

$$\nabla \cdot (\vec{v}(\rho_f E_f + p)) = S_f^h + \nabla \cdot \left[k_{eff}\nabla T - \sum_i h_i J_i + \bar{\tau} \cdot \vec{v}\right] \tag{15}$$

Here E_f stands for the total fluid energy, S_f^h represents the fluid enthalpy source term, and k_{eff} denotes the effective thermal conductivity of the medium.

2.2.3. Solving

In order to achieve reliable CFD simulation results, the high-quality hexahedral structural mesh has been created by using ANSYS ICEM for the computation domain (314 160 cells in total) [35], the outer wall and inlet meshes are presented in Fig. 2(a). The mesh quality assessment in various aspects is shown in Table 1, which proves the feasibility of the mesh for CFD utilization in this study.

After meshing, the CFD model is solved by using ANSYS Fluent 2022 R2 and the mesh independence of the solving problem has been tested first, i.e., compare the simulation results using the current mesh and the refined mesh. The refined mesh is achieved by increasing the number of nodes at each edge by 1.25 times, resulting in 688 505 cells, namely more than twice cell number of the current mesh. Fig. 2(b) compares the NH_3 yield prediction for simulating the same cases (100 bar, temperature range from 370 °C to 430 °C) while using the two kinds of mesh, which shows negligible differences (0.053% difference in average). Thus, considering computational time, the current mesh is implemented for all the simulations in this study. The detailed settings and numerical methods used for the CFD solver are elaborated below.

The key factor of this study, namely the comprehensive kinetic model, is incorporated into ANSYS Fluent via self-defined expressions to describe NH_3 synthesis inside the catalyst bed [36]. The order of the three species is defined as NH_3, H_2 and N_2. Thus, two mass source terms for NH_3 transport equation and H_2 transport equation and one energy source term due to the exothermic reaction are defined in the catalyst zone. The overall mass source term for the continuity equation is set to zero. The SST $k-\omega$ model for modeling turbulence is employed in all simulations to more reliably describe the heat and mass transfer for the near-wall boundary layer regions. The Reynolds number ranges from 3.2×10^3 to 3.7×10^4 for different cases. The y^+ value of walls ranges from 0.3 to 7.3 for the lowest flow rate case, from 2.8 to 59.4 for the highest flow rate case, and the majority of wall y^+ values are below 30. The turbulence model selection in this numerical study considers

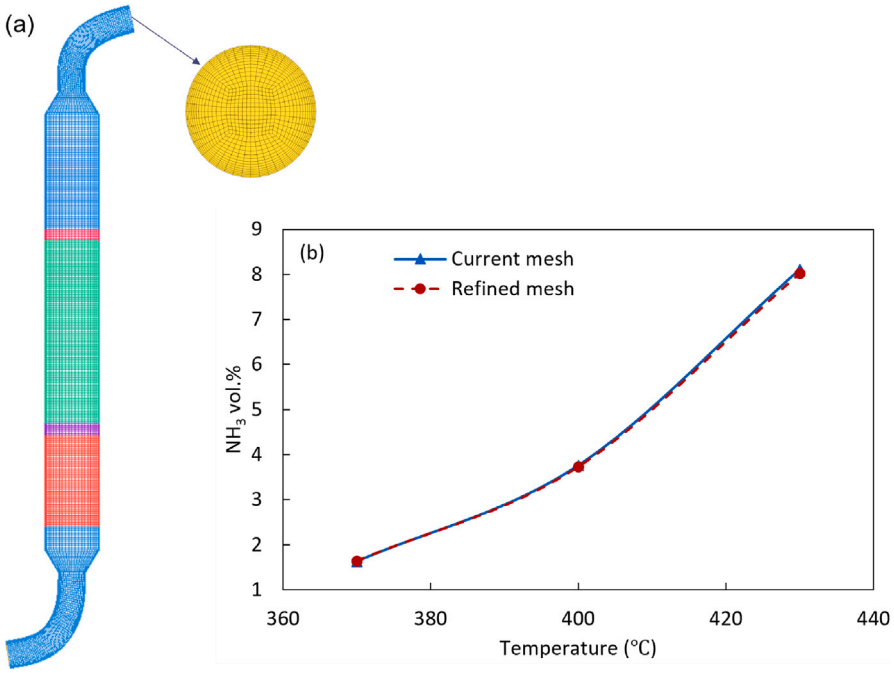

Fig. 2. The hexahedral structural mesh and independence test for the simulated case.

not only unifying the simulation settings but also regarding that the main concern of this work is the catalytic reaction of NH_3 synthesis. The specific models, boundary conditions and numerical methods applied in this CFD simulation are summarized in Table 2.

3. Results and discussion

3.1. Performance of the kinetic model

Before implementing the kinetic model into CFD, the performance of the modified Temkin model over temperature, pressure, H_2/N_2 ratio and NH_3 fraction (conversion) have been assessed, as shown in Fig. 3. Since the kinetic experiments are carried out in the temperature range of 350 °C to 460 °C and pressure range of 50 bar to 100 bar, the performance is mainly assessed in these temperature and pressure ranges. The characteristics of this kinetic model slightly out of the temperature and pressure ranges are also explored, to verify its applicability in broader temperature and pressure ranges. As mentioned in Section 2.1, the reaction rates from the modified Temkin model for various ratios of H_2/N_2 (3 or 1.5) have minor differences [19]. Fig. 3(a) compares the two different reaction rates along temperature under 20 bar, 70 bar, 150 bar and 300 bar with a small NH_3 mole fraction (0.05), which shows that the NH_3 production rates under H_2/N_2 = 1.5 are always gently higher than those under the other ratio if maintaining the same operation conditions. This is attributed to inhibition of the surface catalytic reaction by H_2, hence previous researchers have reported that the Ru catalyst is recommended to be operated in understoichiometric reaction conditions [20].

Fig. 3(b)–(e) present the NH_3 synthesis rate over temperature under 20 bar, 50 bar, 70 bar and 100 bar, respectively. The plots in each subfigures denote the synthesis rates for the mole fraction of NH_3 from 0.05 to 0.8 with a gradient of 0.05, where the blue lines indicate those with positive values and the red dot lines indicate those with negative values. From the results, one can see, first the reaction rate increases along with the rising of temperature and pressure, in which temperature contributes more than pressure. Second pressure significantly affects the chemical equilibrium, at low pressure of 20 bar the synthesis rate will become negative if the NH_3 mole fraction is higher than 0.15, i.e., the synthesis reaction (Eq. (1)) is going to reverse. Whereas, for the pressure at 70 and 100 bar, the critical mole fractions of NH_3 are much higher (0.4 and 0.45, respectively). Fig. 3(f) shows more detailed plots of the reaction rate along temperature for the transition process (from the forward to reverse) under 70 bar, i.e., NH_3 mole fraction from 0.37 to 0.39 with a gradient of 0.005. It can be recognized that the synthesis reaction under high reactants conversion approaches its chemical equilibrium [37]. Several non-linear curves with a clear peak each are observed here for the selected NH_3 mole fractions, illustrating the detailed characteristics and maximum rate of the synthesis reaction at higher conversions.

Fig. 3(g)–(h) displays the NH_3 production rates along the expanding range of temperature (250–500 °C), where Fig. 3(g) compares the differences for a border pressure range (20 bar to 200 bar). The plots are smooth and still maintain the same trends outside of the experimental temperature and pressure ranges, i.e., 350–460 °C and 50–100 bar. Fig. 3(h) presents the NH_3 production rate curves in detail for the transition process under 70 bar, of which the characteristics are consistent with those in Fig. 3(f) that are plotted in the experimental temperature range. Therefore, we conclude that the kinetic model is still reliable in the slightly expanding ranges of temperature and pressure.

In short, several highlights from the kinetic model assessments can be conducted:

- The synthesis rates for H_2/N_2 = 1.5 are gently higher than those for H_2/N_2 = 3 if the other conditions are the same, while the trends for the two rates along temperature and pressure are consistent with each other.
- The synthesis process is a forward reaction, i.e., producing NH_3, at relatively lower NH_3 fractions or reactant conversions.
- The synthesis rate is more sensitive to temperature than pressure, temperature increase would significantly raise the reaction rate.
- The pressure affects the chemical equilibrium a lot and moderately influences the reaction rate.
- The kinetic model is still applicable in broader temperature and pressure ranges other than that of the carried out experiments.

Table 3
Simulated cases for validation in this study from [19].

Case	Temperature (°C)	Pressure (bar)	H_2/N_2 vol.
1	430	100	3
2	430	70	3
3	370	100	3
4	370	85	3
5	430	85	3
6	370	70	3
7	430	100	1.5
8	430	70	1.5
9	370	100	1.5
10	370	85	1.5
11	430	85	1.5
12	400	50	1.5

3.2. Model validation

For the purpose of validation, the isothermal simulation has been conducted first to compare with the experimental data, for which the operation conditions are listed in Table 3. For the conducted isothermal experiments, the temperature varies from 370 °C to 430 °C, pressure ranges from 50 bar to 100 bar, the ratio of H_2/N_2 equals to 3 (Case 1–6) or 1.5 (Case 7–12) [19] and the space velocity distributes from 50 000 h^{-1} to 400 000 h^{-1}. Then, the non-isothermal simulation has been carried out to demonstrate and better analyze the catalytic synthesis of NH_3 in a real lab demonstrator. The only difference between the isothermal simulation and the non-isothermal simulation is the way of modeling the thermal energy in the catalyst zone. The former assumes a fixed temperature (consistent with the corresponding experiment) for the whole porous zone, and the latter uses a fixed temperature as the thermal boundary condition of the sidewalls and solves a lumped energy transport equation (Eq. (15)) in the catalyst zone. Both the isothermal simulation and non-isothermal simulation are executed under the same experimental conditions for every validation case. The operation conditions specified in CFD are described in Table 4.

3.2.1. Isothermal simulation

Fig. 4 presents the validation results, where Fig. 4(a) and (c) compare the simulation results with experimental data along GHSV for the cases under H_2/N_2 equals to 3 or 1.5, respectively. And Fig. 4(b) and (d) show the parity plots of the measured data and modeling results presented in Fig. 4a and c, respectively. From the comparison results, the following consequences can be obtained. First, the simulation results overall agree well with the measured data and show the same trends with the experimental results, i.e., NH_3 production is boosted as the temperature and/or pressure increases while reduced as the GHSV increases. Second, the comparison between simulations and experiments for the cases of $H_2/N_2 = 3$ performs better than that for the cases of $H_2/N_2 = 1.5$, mainly owing to the large comparison differences for Case 7. Third, the simulation-experiment variations are bigger for the cases with higher temperatures. It is probably due to the kinetic model being very sensitive to temperature, and the tiny experimental error would be magnified for high temperature condition. In practice, the temperature gradient should exist in the catalyst zone for the high flow rate cases instead of fully isothermal, even though the relevant actions have been taken to keep temperature uniform in these experiments.

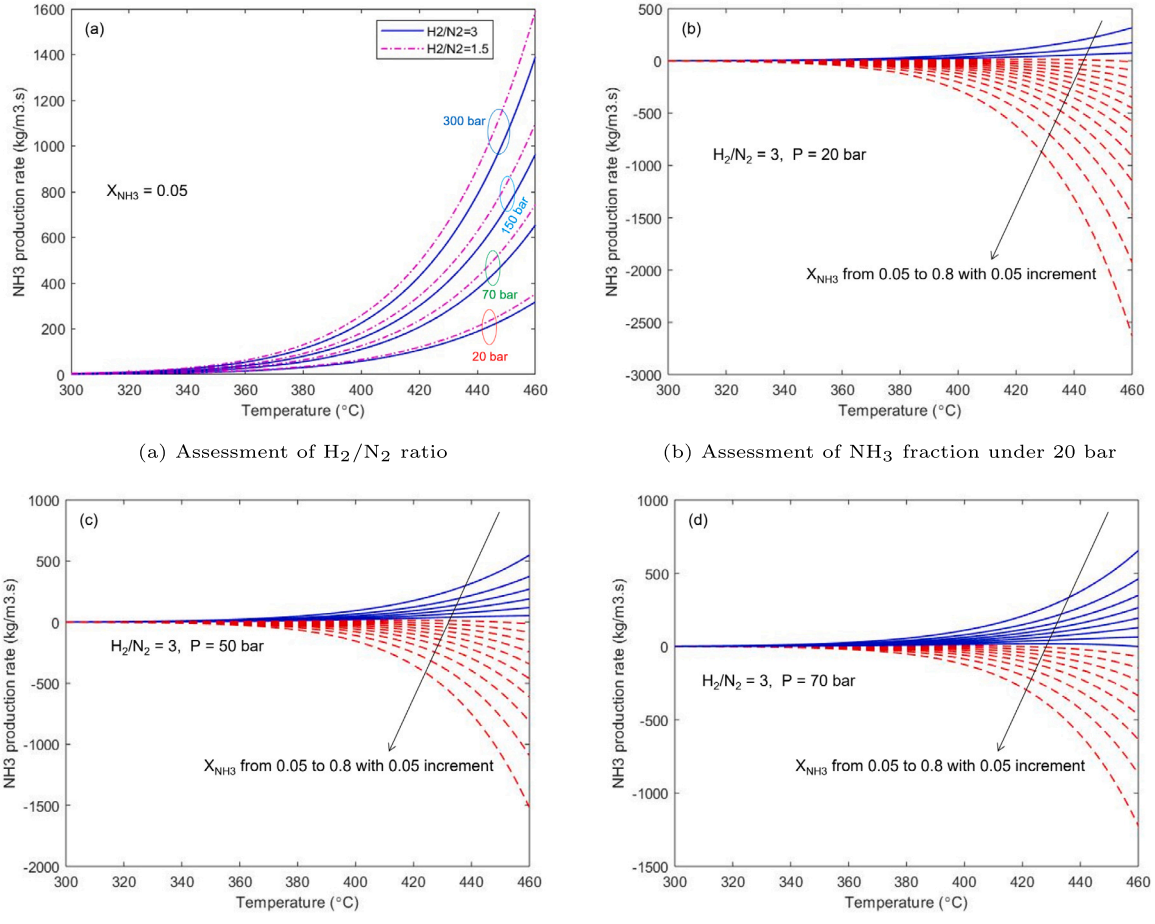

(a) Assessment of H_2/N_2 ratio

(b) Assessment of NH_3 fraction under 20 bar

(c) Assessment of NH_3 fraction under 50 bar

(d) Assessment of NH_3 fraction under 70 bar

Fig. 3. Performance of the kinetic models in terms of pressure, temperature, ratio of H_2 to N_2 and NH_3 mole fraction.

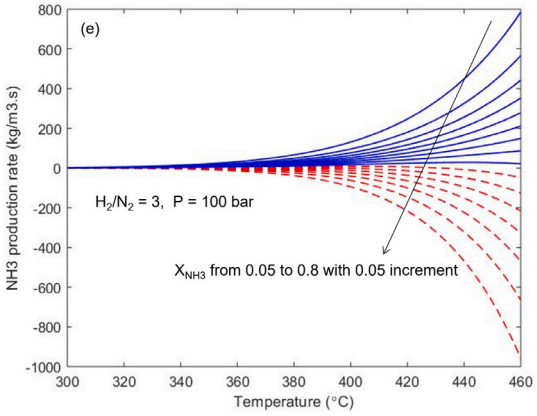

(e) Assessment of NH_3 fraction under 100 bar

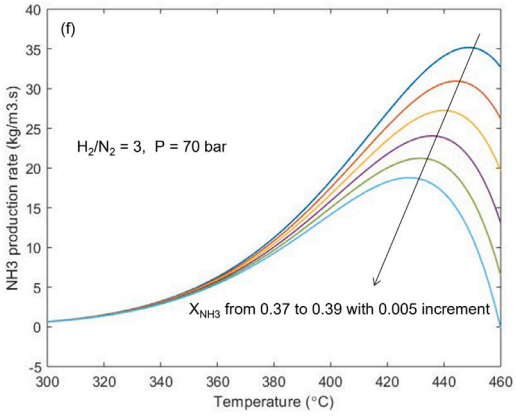

(f) Assessment of high conversion

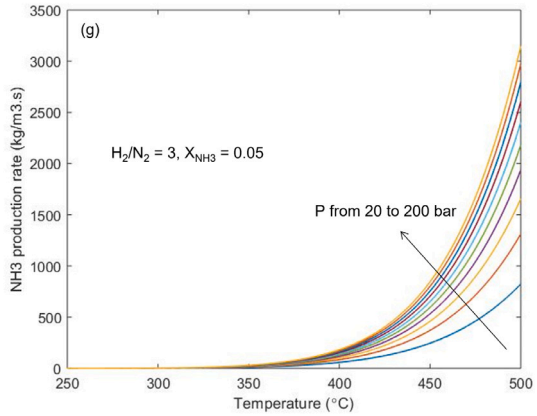

(g) Assessment of wider pressure and temp. range

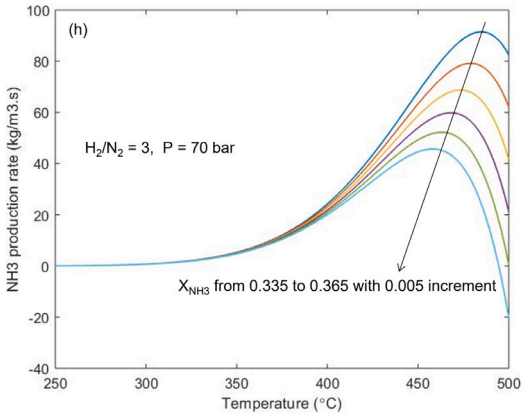

(h) Assessment of high conversion in wider temp. range

Fig. 3. (*continued*).

Table 4
Operation conditions used in CFD of this study.

Operation conditions	Description
Operating pressure	Consistent with corresponding experimental case
Wall boundary	Catalyst bed wall: fixed temperature, consistent with experimental case; Other walls: adiabatic
Inlet mass flow	Calculated based on the GHSV, ranging from 1.02 to 8.16 g/s for H_2/N_2 = 1.5, 0.7 to 5.6 g/s for H_2/N_2 = 3 along 50 000–400 000 h^{-1} GHSV
Porous zone	Isothermal simulation: fixed temperature, consistent with experimental case; Non-isothermal simulation: solve one lumped energy equation
Outlet temperature	Consistent with its corresponding experimental case, only used for reverse flow
Inlet temperature	300 K

To verify the universality of the model, experimental data using other Ru-based catalysts under 100 bar, GHSV = 10 000 h^{-1} and 375–400 °C temperature range have also been compared with the simulation results, as shown in Fig. 5. The preparation and properties of the catalysts refer to [38]. The reasonable results (values and trends) of NH_3 production using various Ru-based catalysts have been speculated from the current CFD model. In detail, the simulated NH_3 fractions are close to the experimental data for the temperature at 375 °C and 400 °C, while a larger difference is observed at 425 °C. Apart from the sensitivity of the kinetic model at high temperature, another interpretation can be that the kinetics for Ru/C catalyst used in the CFD simulation is not completely suitable for the other Ru-based catalyst. The performances of different Ru-based catalysts for NH_3 synthesis can also vary significantly. The comparison proves that the developed CFD model is comprehensive and can be generally applied in NH_3 synthesis for giving out reasonable results, while the specific kinetics for the corresponding catalyst are still needed to deliver more accurate results.

3.2.2. Non-isothermal simulation

Even though the isothermal CFD simulation has been well established, the non-isothermal simulation is still necessary for investigating NH_3 synthesis [39]. Owing to the exothermic reaction and fluid flow, it is not an isothermal process for a real lab-scale demonstrator of NH_3 synthesis. Fig. 6(a) compares the non-isothermal simulation and isothermal simulation with measured data, in which GHSV = 60 000 h^{-1} (60 kSV) and 12 000 h^{-1} (120 kSV) are chosen as the inlet flow for all the cases. Overall, the result shows that non-isothermal simulation results are very close to the isothermal simulation results and also show good agreements with the experimental data. While the non-isothermal simulation is always underestimated compared to the isothermal simulation, mainly due to the temperature gradient inside the catalyst bed [40]. As shown in Fig. 6(b), a thermal comparison example, clearly displays thermal gradients inside the reactor for non-isothermal simulation, whereas the temperature in the catalyst zone is uniform for the isothermal simulation. The volume-averaged temperature for the presented non-isothermal simulation is 415.5 °C, which is lower than the experimental and the isothermal simulation temperature, i.e., 430 °C. In addition, the comparison between simulation and experiment performs better for higher space velocity and lower temperature, owing to the properties of the kinetic model. Hence we conclude that the non-isothermal simulation for the lab-scale reactor is also validated.

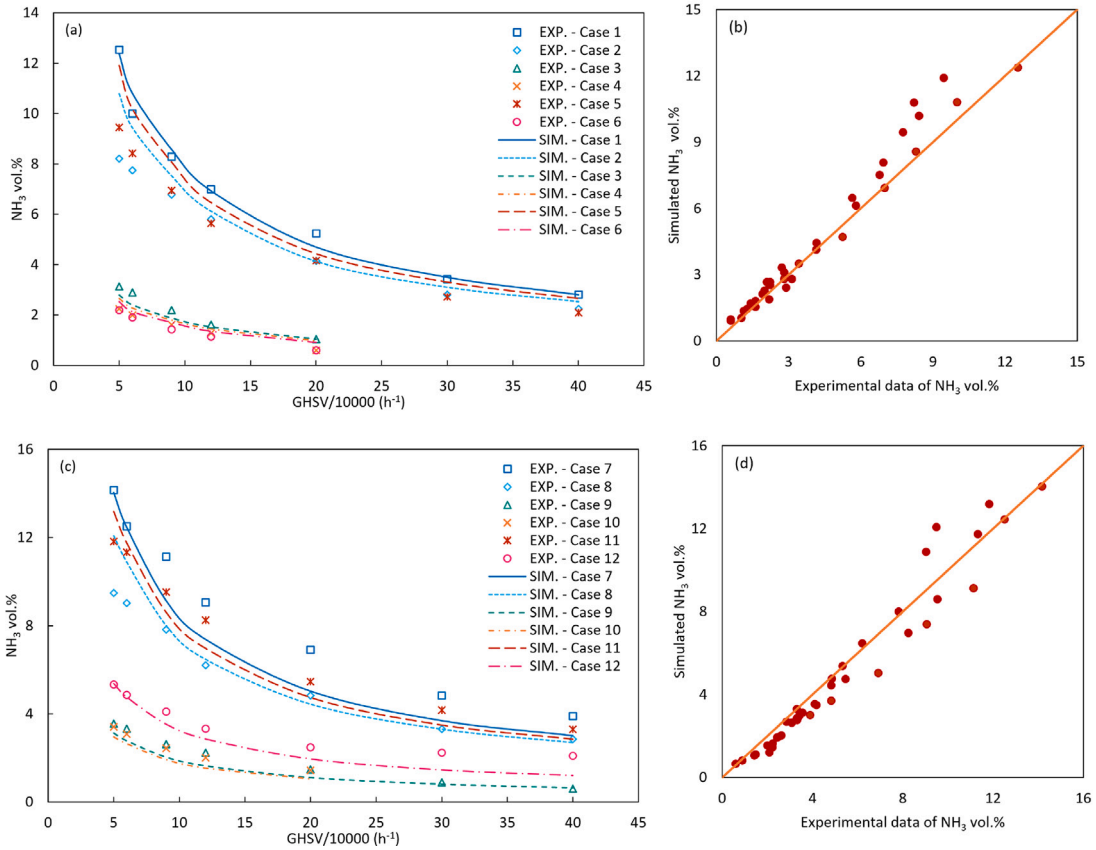

Fig. 4. Comparison of CFD results with experimental data in [19] using Ru/C catalyst.

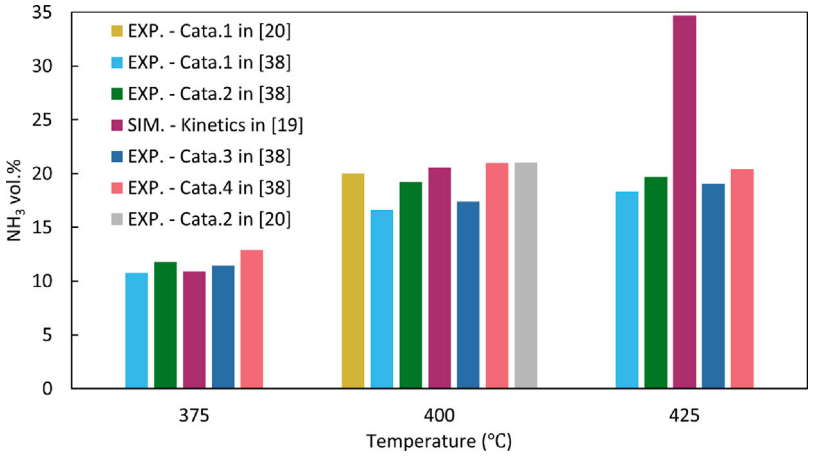

Fig. 5. Comparison of the CFD results with other experimental data.

A detailed case analysis (Case 2 with 12 000 h^{-1} GHSV) based on the non-isothermal CFD simulation is presented below.

Fig. 7(a)–(c) show the contours of temperature (a), H_2 mass fraction (b) and NH_3 mass fraction (c) in the XZ middle plane of the reactor, from which the following consequences are concluded. First, the distributions of temperature and the two species along the flow direction are captured. The three variables remain the initial values before the fluid flow enters into the catalyst bed. Then the temperature and NH_3 mass fraction continually increase and the reactant H_2 decreases in the catalyst bed due to the synthesis reaction. Afterwards, the gas mixture flows into the non-catalyst tube and finally goes out at the outlet surface without significant changes in terms of temperature and species. Second, clear thermal gradient and species gradients along the reactor diameter are observed. At the half-top part of the catalyst bed, the sidewall temperature (430 °C) is higher than the reacting flow temperature, resulting in the produced NH_3 near the sidewall being more than that in the middle. Here, the sidewalls are 'heating' walls, which provide a fixed temperature heating source. Along with heating up the fluid flow, the catalytic reaction becomes more intensive, which consumes more reactants and yields a large amount of NH_3 and heat. Gradually the sidewall temperature is lower than the temperature in the middle at the bottom part of the catalyst bed, where the sidewalls becomes 'cooling' walls. Afterwards, the high-temperature effluent gas gets out from the outlet surface.

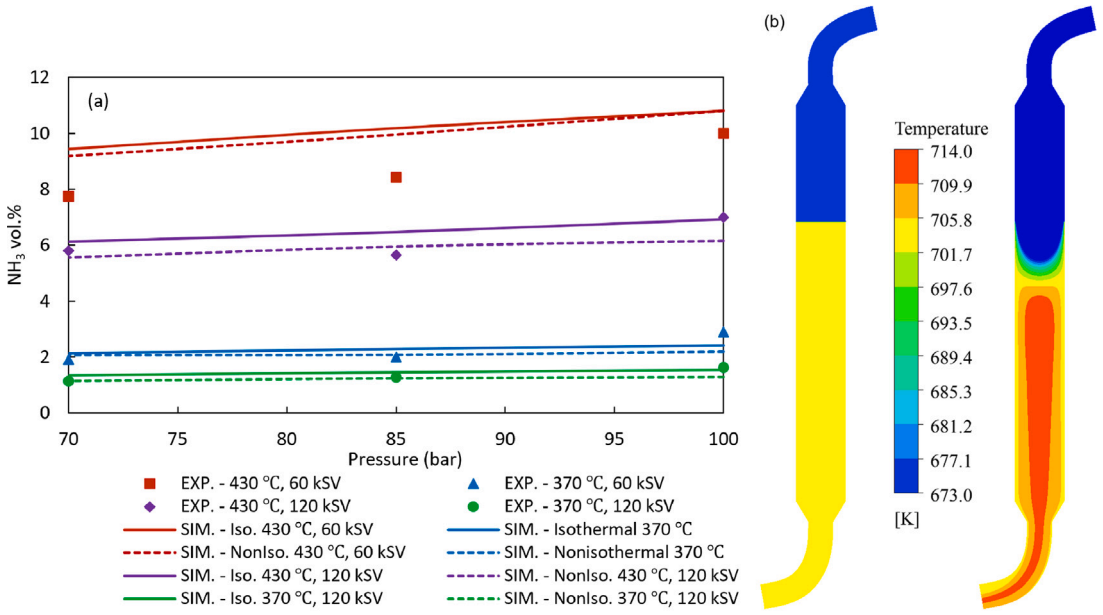

Fig. 6. Comparison of the non-isothermal simulation with isothermal simulation and experimental data under 85 bar (a) and the temperature contours of the non-isothermal simulation with isothermal simulation for Case 5 (b).

To better view the synthesis process inside the catalyst bed, Fig. 7(d)–(f) display the contours of temperature (d), NH_3 mass fraction (e) and H_2 mass fraction (f) in the five XY planes at different heights (10 mm gradient) of the bed including its top and bottom surfaces. The nearly uniform thermal and species gradients along the cylindrical reactor diameter are observed. Specifically, the temperature near the wall is higher than that in the 1/4 top part, while it is the opposite in the 3/4 bottom part. The H_2 consumption and NH_3 production are consistent with the thermal gradient tendency and opposite to each other. The area-weighted averaged temperature, mass fraction of H_2 and NH_3 at the outlet surface are 433.86 °C, 15.89% and 10.52%, respectively.

Shortly, the CFD model with an isothermal catalytic reaction zone is validated by the experimental data using various Ru-based catalysts from different references, in which 94 cases in wide ranges of pressure, temperature and mass flow rate have been compared with. Then, the full non-isothermal CFD model which more practically simulates the lab-scale demonstrator of NH_3 synthesis, is likewise validated by the measurement data and compared with the isothermal simulation. The minor comparison difference and logical simulation results inside the reactor have highlighted the reliability and applicability of the CFD model.

3.3. Parametric study

To further investigate NH_3 synthesis on Ru-based catalyst, parametric studies based on the non-isothermal CFD simulation for the lab reactor have been carried out in this section. The impacts of temperature and flow rate which are the top two sensitive factors for NH_3 synthesis are explored as follows.

3.3.1. Impacts of temperature

Fig. 8 illustrates the synthetic NH_3 volume fraction at the outlet (a) and the volume-averaged NH_3 synthesis rate in the catalysts bed (b) over temperature range of 370 °C to 430 °C with 15 °C gradient at pressure of 70 bar and 85 bar. First, the NH_3 production and the reaction rate increase near exponentially along the temperature rise, thanks to the exponential function of the kinetic model in terms of temperature. The average reaction rate is boosted 4–5 times for a 60 °C temperature rise (from 370 °C to 430 °C). Second, 15 bar pressure increase does not affect the reaction rate and NH_3 production significantly compared to temperature, while the impact due to pressure change can be enlarged under a high temperature condition as compared in Fig. 8(b). It is reasonably believed that the larger difference is attributed to the sensitivity of the reaction rate to temperature.

To analyze the reaction process more deeply, the distributions of NH_3 synthesis rate inside the catalyst bed under 430 °C (a,b), 400 °C (c,d) and 370 °C (e,f) are compared in Fig. 9, where Fig. 9(a, c, e) show the results for 85 bar, and the other three show the results for 70 bar. The contours derived from the same temperature cases (e.g., (a) and (b)) share the same color bar. The results prove that the maximum reaction rate occurs near the sidewall when the reactants enter into the catalyst bed due to the hot wall temperature and the very low NH_3 concentration, resulting in apparent gradients from the top sidewall to the other zone. For example, as shown in Fig. 9(a) the reaction rate is up to 115.37 $kg/(m^3\,s)$ near the initial sidewall, while the NH_3 production rate for the whole catalyst bed is in the range of 20–60 $kg/(m^3\,s)$ for the case under 430 °C and 85 bar. The maximum rates for the six cases are verified from tens to hundreds $kg/(m^3\,s)$, mainly owing to the differences in temperature. Along the flow direction, reactants are continuously heating up by the sidewall and the heat produced by the exothermic reaction even surpass the fixed wall temperature, gradually raising the rates in the middle over those near the wall. Afterwards, the hot fluid flow is cooled down by the bottom part of the sidewall and the produced NH_3 is constantly accumulated, resulting in the reaction rate decrease in the bed bottom part and finally forming a triangle intensive-reaction zone. The triangle zone of the case under 85 bar is always bigger than the corresponding case under 70 bar, probably due to higher pressure favoring the equilibrium as aforementioned in Section 3.1.

3.3.2. Impacts of GHSV

Fig. 10 shows the mass fraction of NH_3 at the outlet (a) under 70 bar and 400 °C and 430 °C, respectively, along GHSV from 60 000 h^{-1} to 300 000 h^{-1} with the gradient of 30 000 h^{-1}. First, the produced NH_3 volume fraction and the production rate fall with the increase in GHSV. And the falling gradients at lower GHSV (e.g., from 60 000 h^{-1} to 90 000 h^{-1}) are larger than those at higher GHSV. Two main factors contribute to this phenomenon, one is the big GHSV means a

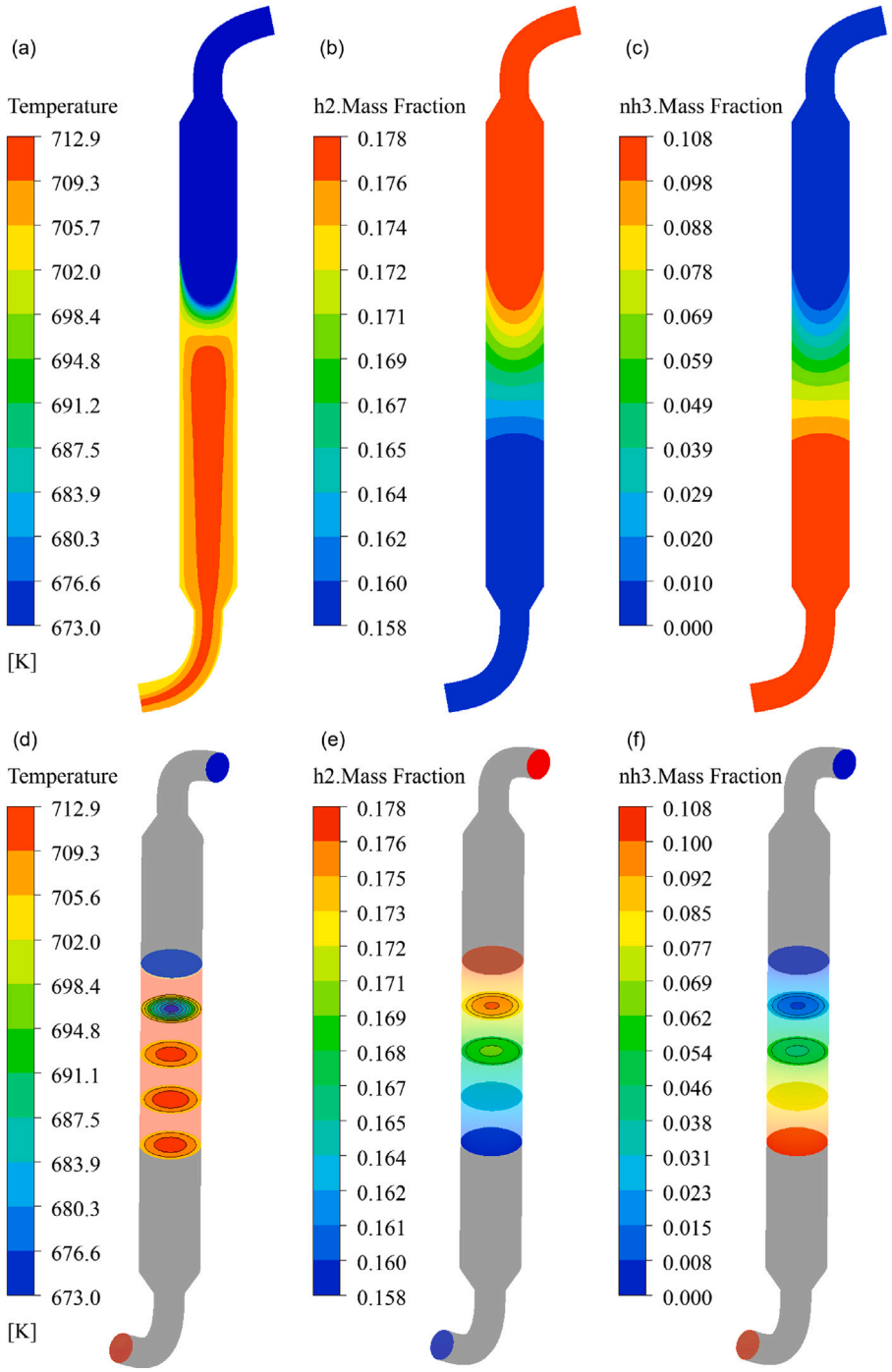

Fig. 7. CFD simulated contours of temperature and mass fractions of H_2 and NH_3 inside the reactor.

large amount of thermal mass, which is hard to be heated up in the bed for the catalytic reaction. The other reason is the high velocity of the fluid flow for the big GHSV cases, which leads to the short residence time of the reactants in the reaction bed. Second, a significant difference due to temperature variation is observed, while the difference is weakened along the space velocity increase. It can be explained that the difficulties in heating up large thermal mass for high GHSV hinder the catalytic reaction to some extent.

To eliminate the difference of NH_3 production due to mass flow variation, and therefore better analyze the impacts of GHSV, the generalized NH_3 production rate or NH_3 productivity in terms of catalyst volume is calculated using the below expression.

$$r_{NH_3} = GHSV \cdot \rho_{flow} \cdot Y_{NH_3} \tag{16}$$

where r_{NH_3} is the generalized production rate with the unit $kg/(m^3_{cat}\ h)$, ρ_{flow} denotes the density of the fluid flow, and Y_{NH_3} indicates the mass fraction of NH_3 at the outlet. Fig. 10(b) displays the average NH_3 production rate (left Y axial) and the defined NH_3 productivity (right Y axial) along GHSV for the two cases under 70 bar. From the results, one can see, that the production rate and its corresponding productivity show the same tendency along GHSV, i.e., increase first and then decrease. Therefore, the best GHSV in terms of the two production rates is found, namely 180 000 h^{-1}, both for the two cases under different 430 °C and 400 °C. The operation with low GHSV (e.g., 60 000 h^{-1})

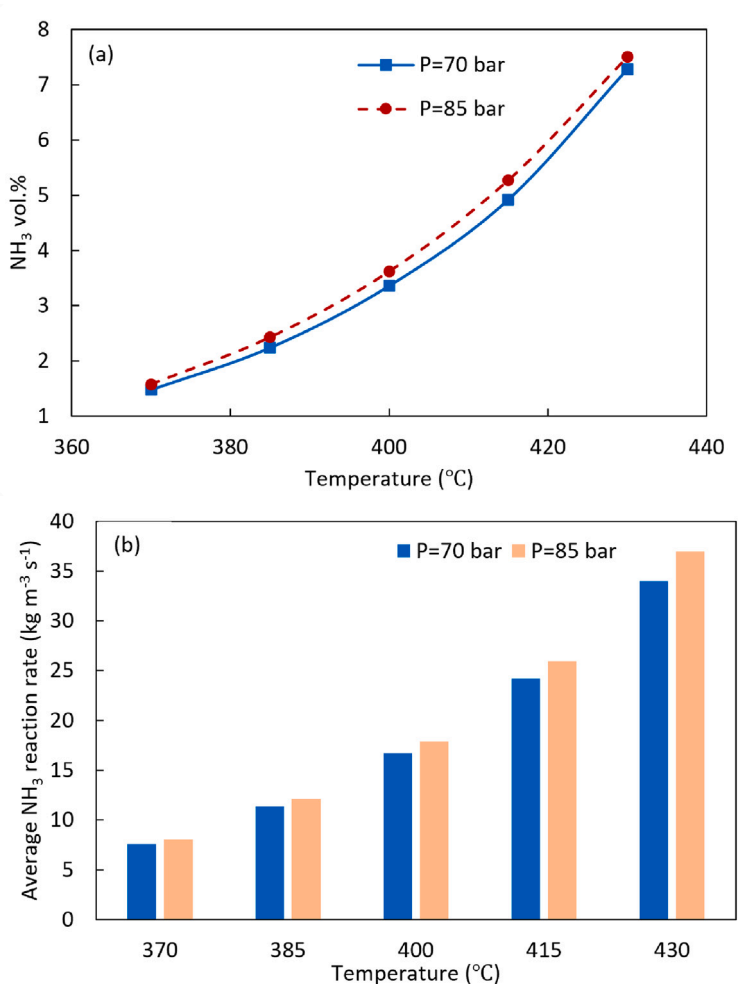

Fig. 8. NH_3 fractional yields (a) and average production rates (b) under different temperatures.

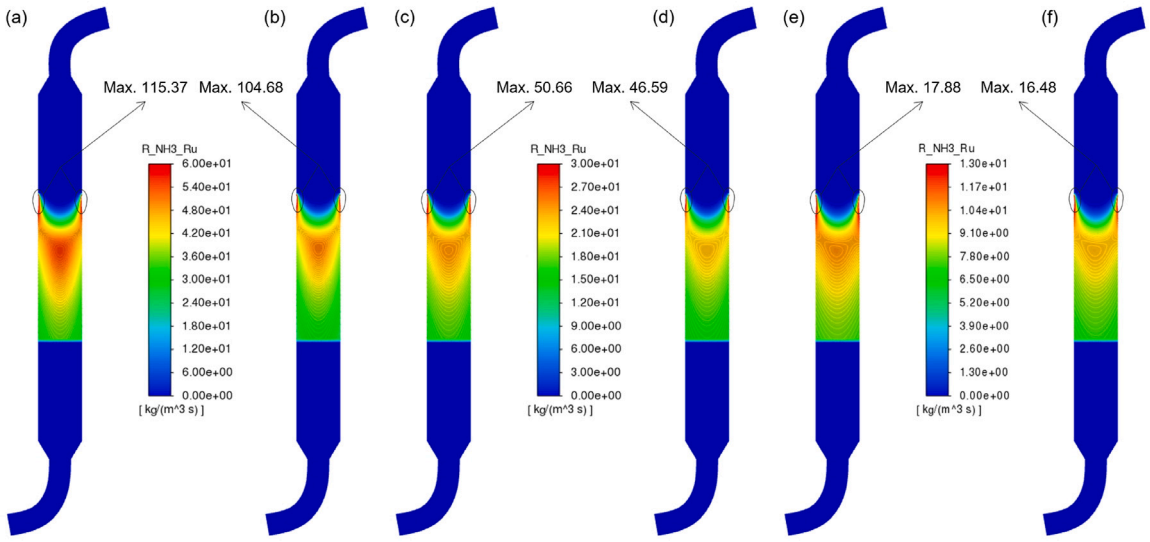

Fig. 9. Contours of NH_3 production rate in the middle plane of the catalytic reactor: (a) 430 °C, 85 bar (b) 430 °C, 70 bar (c) 400 °C, 85 bar (d) 400 °C, 70 bar (e) 370 °C, 85 bar (f) 370 °C, 70 bar.

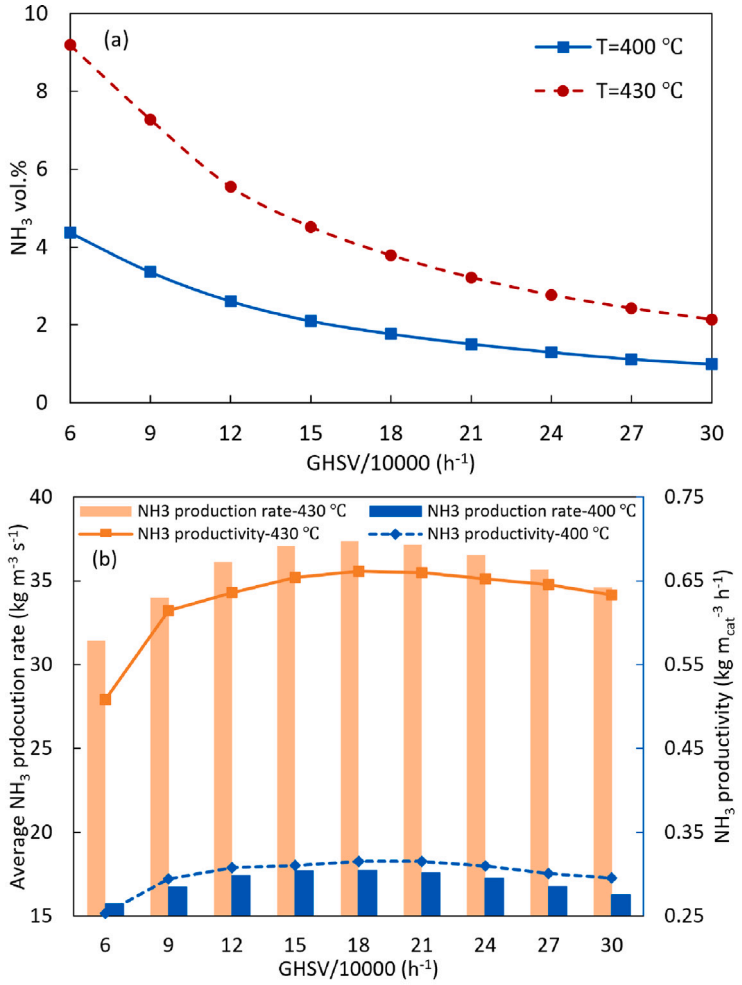

Fig. 10. NH_3 fractional yields (a) and average production rates with the productivities (b) along GHSV.

provides particularly poor performance for NH_3 productivity. Moreover, in contrast with space velocity temperature is still the dominant factor for NH_3 production. The generalized production rates of NH_3 under 430 °C are more than two times larger than those under the operation temperature 30 °C lower. These interesting results are of great importance to control and optimize the similar reactor for NH_3 synthesis.

4. Conclusions

This paper presents a comprehensive study on compact NH_3 synthesis (Haber–Bosch process) using Ru-based catalysts under mild operating conditions. A CFD model has been developed and validated by comparing with experimental data, which incorporates an up-to-date kinetic model describing the complex catalytic reaction. The universality of the model has been verified through simulations on other Ru-based catalysts as well. The simulation results provide valuable insights into the NH_3 synthesis process, such as the distributions of temperature and species inside the reactor, thermal gradient and species variation along the flow direction, and the sensitivity of the synthesis process to various parameters. Through CFD-based parametric studies, the significant impacts of temperature and space velocity on NH_3 production and heat and mass transfer inside the catalyst bed have been quantitatively revealed. The results show that temperature influences NH_3 production most, i.e., more than two times due to 30 °C variation, while pressure dominates the chemical equilibrium (or maximum conversion), verifying the efficiency of moderate temperature and low pressure operation conditions. The effect modes of space velocity on NH_3 production are exposed, i.e., thermal mass heating and the residence time which suggest the best gas hourly space velocity, namely 180 000 h^{-1} in terms of NH_3 productivity. The findings presented in this paper offer useful guidelines for designing and optimizing decentralized NH_3 synthesis reactor and demonstrate the potential of CFD modeling as a powerful tool for understanding, improving, and controlling decentralized NH_3 synthesis process.

CRediT authorship contribution statement

Tianbao Gu: Conceptualization, Methodology, Visualization, Writing – original draft. **Samuel Simon Araya:** Conceptualization, Writing – review & editing. **Chungen Yin:** Supervision, Writing – review & editing. **Vincenzo Liso:** Funding acquisition, Project Administration, Conceptualization, Writing – review & editing.

Declaration of competing interest

The authors declare that they have no known competing financial interests or personal relationships that could have appeared to influence the work reported in this paper.

Data availability

Data will be made available on request.

Acknowledgments

This work was supported by the European Union – Horizon Europe, Grant Agreement [101058643], HySTrAm : Hydrogen Storage and Transport using Ammonia.

References

[1] IEA. Net zero by 2050: A roadmap for the global energy sector. 2021.
[2] Del Pozo CA, Cloete S. Techno-economic assessment of blue and green ammonia as energy carriers in a low-carbon future. Energy Convers Manage 2022;255:115312. http://dx.doi.org/10.1016/j.enconman.2022.115312.
[3] Berwal P, Kumar S, Khandelwal B. A comprehensive review on synthesis, chemical kinetics, and practical application of ammonia as future fuel for combustion. J Energy Inst 2021;99:273–98. http://dx.doi.org/10.1016/j.joei.2021.10.001.
[4] Incer-Valverde J, Patiño-Arévalo LJ, Tsatsaronis G, Morosuk T. Hydrogen-driven Power-to-X: State of the art and multicriteria evaluation of a study case. Energy Convers Manage 2022;266:115814. http://dx.doi.org/10.1016/j.enconman.2022.115814.
[5] Chiuta S, Everson RC, Neomagus HW, Bessarabov DG. Hydrogen production from ammonia decomposition over a commercial Ru/Al2O3 catalyst in a microchannel reactor: Experimental validation and CFD simulation. Int J Hydrogen Energy 2016;41(6):3774–85. http://dx.doi.org/10.1016/j.ijhydene.2015.12.130.
[6] Zhou D, Zhou R, Zhou R, Liu B, Zhang T, Xian Y, Cullen PJ, Lu X, Ostrikov KK. Sustainable ammonia production by non-thermal plasmas: Status, mechanisms, and opportunities. Chem Eng J 2021;421:129544. http://dx.doi.org/10.1016/j.cej.2021.129544.
[7] Smith C, Hill AK, Torrente-Murciano L. Current and future role of Haber–Bosch ammonia in a carbon-free energy landscape. Energy Environ Sci 2020;13(2):331–44. http://dx.doi.org/10.1039/C9EE02873K.
[8] Nowicki DA, Agnew GD, Irvine JT. Green ammonia production via the integration of a solid oxide electrolyser and a Haber-Bosch loop with a series of solid electrolyte oxygen pumps. Energy Convers Manage 2023;280:116816. http://dx.doi.org/10.1016/j.enconman.2023.116816.
[9] Movick WJ, Kishimoto F, Takanabe K. Dynamic surface-coverage alteration based on microkinetic analysis for enhanced ammonia synthesis over ruthenium catalysts at low temperatures. Chem Eng J 2023;452:139525. http://dx.doi.org/10.1016/j.cej.2022.139525.
[10] Dowden D. Catalytic ammonia synthesis: Fundamentals and practice. Springer Science & Business Media; 1991.
[11] Zhang T, Miyaoka H, Miyaoka H, Ichikawa T, Kojima Y. Review on ammonia absorption materials: metal hydrides, halides, and borohydrides. ACS Appl Energy Mater 2018;1(2):232–42. http://dx.doi.org/10.1021/acsaem.7b00111.
[12] MacFarlane DR, Cherepanov PV, Choi J, Suryanto BH, Hodgetts RY, Bakker JM, Vallana FMF, Simonov AN. A roadmap to the ammonia economy. Joule 2020;4(6):1186–205. http://dx.doi.org/10.1016/j.joule.2020.04.004.
[13] van Raak T, Li S, Gallucci F. Prevailing surface reactions in the plasma-catalytic ammonia synthesis with Ru/CeO2 and Ru/Ti-CeO2. Chem Eng J 2023;455:140691. http://dx.doi.org/10.1016/j.cej.2022.140691.
[14] Liang C, Wei Z, Xin Q, Li C. Ammonia synthesis over Ru/C catalysts with different carbon supports promoted by barium and potassium compounds. Appl Catal A: Gen 2001;208(1–2):193–201. http://dx.doi.org/10.1016/S0926-860X(00)00713-4.
[15] Hinrichsen O. Kinetic simulation of ammonia synthesis catalyzed by ruthenium. Catal Today 1999;53(2):177–88. http://dx.doi.org/10.1016/S0920-5861(99)00115-7.
[16] Smith C, Torrente-Murciano L. Exceeding single-pass equilibrium with integrated absorption separation for ammonia synthesis using renewable energy—Redefining the Haber-Bosch loop. Adv Energy Mater 2021;11(13):2003845. http://dx.doi.org/10.1002/aenm.202003845.
[17] Nikačević N, Jovanović M, Petkovska M. Enhanced ammonia synthesis in multifunctional reactor with in situ adsorption. Chem Eng Res Des 2011;89(4):398–404. http://dx.doi.org/10.1016/j.cherd.2010.08.011.
[18] Nielsen A, Kjaer J, Hansen B. Rate equation and mechanism of ammonia synthesis at industrial conditions. J Catalysis 1964;3(1):68–79. http://dx.doi.org/10.1016/0021-9517(64)90094-6.
[19] Rossetti I, Pernicone N, Ferrero F, Forni L. Kinetic study of ammonia synthesis on a promoted Ru/C catalyst. Ind Eng Chem Res 2006;45(12):4150–5. http://dx.doi.org/10.1021/ie051398g.
[20] Tripodi A, Compagnoni M, Bahadori E, Rossetti I. Process simulation of ammonia synthesis over optimized Ru/C catalyst and multibed Fe+ Ru configurations. J Ind Eng Chem 2018;66:176–86. http://dx.doi.org/10.1016/j.jiec.2018.05.027.
[21] Versteeg HK, Malalasekera W. An introduction to computational fluid dynamics: The finite volume method. Pearson education; 2007.
[22] Nikzad A, Iranshahi D, Ranjbaran M, Bagherpour-Ardakani E. Conceptual comparison of three novel configurations in the spherical radial flow reactor for ammonia production. Fuel 2022;321:123945. http://dx.doi.org/10.1016/j.fuel.2022.123945.
[23] Mirvakili A, Eksiri Z, Biniaz P, Mohaghegh N. Two-dimensional mathematical modeling of an industrial ammonia synthesis reactor with CFD analysis. J Taiwan Inst Chem Eng 2021;121:1–19. http://dx.doi.org/10.1016/j.jtice.2021.03.032.
[24] Brown DE, Edmonds T, Joyner RW, McCarroll JJ, Tennison SR. The genesis and development of the commercial BP doubly promoted catalyst for ammonia synthesis. Catal Lett 2014;144:545–52. http://dx.doi.org/10.1007/s10562-014-1226-4.
[25] Annable D. Application of the Temkin kinetic equation to ammonia synthesis in large-scale reactors. Chem Eng Sci 1952;1(4):145–54. http://dx.doi.org/10.1016/0009-2509(52)87011-3.
[26] Dyson D, Simon J. Kinetic expression with diffusion correction for ammonia synthesis on industrial catalyst. Ind Eng Chem Fundam 1968;7(4):605–10. http://dx.doi.org/10.1021/i160028a013.
[27] Ferraris GB, Donati G, Rejna F, Carra S. An investigation on kinetic models for ammonia synthesis. Chem Eng Sci 1974;29(7):1621–7. http://dx.doi.org/10.1016/0009-2509(74)87013-2.
[28] Suhan MBK, Hemal MNR, Choudhury MS, Mazumder MAA, Islam M. Optimal design of ammonia synthesis reactor for a process industry. J King Saud Univ, Eng Sci 2022;34(1):23–30. http://dx.doi.org/10.1016/j.jksues.2020.08.004.
[29] Maleki H, Fulton M, Bertola V. Kinetic assessment of H2 production from NH3 decomposition over CoCeAlO catalyst in a microreactor: Experiments and CFD modelling. Chem Eng J 2021;411:128595. http://dx.doi.org/10.1016/j.cej.2021.128595.
[30] Bian Z, Xia H, Zhong W, Jiang B, Yu Y, Wang Z, Yu K. CFD simulation on hydrogen-membrane reactor integrating cyclohexane dehydrogenation and CO2 methanation reactions: A conceptual study. Energy Convers Manage 2021;235:113989. http://dx.doi.org/10.1016/j.enconman.2021.113989.
[31] Gu T, Yin C, Ma W, Chen G. Municipal solid waste incineration in a packed bed: A comprehensive modeling study with experimental validation. Appl Energy 2019;247:127–39. http://dx.doi.org/10.1016/j.apenergy.2019.04.014.
[32] Liu H. Ammonia synthesis catalysts: Innovation and practice. World Scientific; 2013.
[33] Ansys. ANSYS fluent theory guide release 2021 R1. ANSYS Inc.; 2021.
[34] Ansys. Ansys fluent user's guide release 2021 R1. ANSYS Inc.; 2021.
[35] Ansys. ANSYS ICEM CFD user's manual release 2021 R1. ANSYS Inc.; 2021.
[36] Ansys. ANSYS fluent customization manual release 2021 R1. ANSYS Inc.; 2021.
[37] Pernicone N, Ferrero F, Rossetti I, Forni L, Canton P, Riello P, Fagherazzi G, Signoretto M, Pinna F. Wustite as a new precursor of industrial ammonia synthesis catalysts. Appl Catal A: Gen 2003;251(1):121–9. http://dx.doi.org/10.1016/S0926-860X(03)00313-2.
[38] Jun N, Rong W, Fanhua K, ZHANG T, Jianxin L, Kemei W, et al. Highly efficient Ru-Ba/AC catalyst promoted by magnesium for ammonia synthesis. Chin J Catal 2011;32(3–4):436–9. http://dx.doi.org/10.1016/S1872-2067(10)60179-9.
[39] Liebner C, Wolf D, Baerns M, Kolkowski M, Keil FJ. A high-speed method for obtaining kinetic data for exothermic or endothermic catalytic reactions under non-isothermal conditions illustrated for the ammonia synthesis. Appl Catal A: Gen 2003;240(1–2):95–110. http://dx.doi.org/10.1016/S0926-860X(02)00415-5.
[40] Hayes RE, Kolaczkowski ST. Mass and heat transfer effects in catalytic monolith reactors. Chem Eng Sci 1994;49(21):3587–99. http://dx.doi.org/10.1016/0009-2509(94)00164-2.